Competing Channels in the Thermal Decomposition of Azidoacetone Studied by Pyrolysis in Combination with Molecular Beam Mass Spectrometric Techniques

Patrick O'Keeffe,[†] Giorgio Scotti,[†] Domenico Stranges,*[,†,#] Paula Rodrigues,[‡] M. Teresa Barros,[‡] and Maria L. Costa[§]

Dipartimento di Chimica, Università "La Sapienza", P.le A. Moro 5, Rome I-00185, Italy, ISMN-CNR, Sez. Roma 1, P. le A. Moro 5, Rome I-00185, Italy, REQUIMTE, CQFB, Centro de Química Fina e Biotecnologia, Departamento de Química, Faculdade de Ciências e Tecnologia, Universidade Nova de Lisboa, Quinta da Torre, 2829-516, Caparica, Portugal, and Departamento de Física, Faculdade de Ciências e Tecnologia, Universidade Nova de Lisboa, Quinta da Torre, 2829-516, Caparica, Portugal

Received: September 14, 2007; In Final Form: November 12, 2007

The thermal decomposition of azidoacetone ($CH_3COCH_2N_3$) was studied using a combined experimental and computational approach. Flash pyrolysis at a range of temperatures (296−1250 K) was used to induce thermal decomposition, and the resulting products were expanded into a molecular beam and subsequently analyzed using electron bombardment ionization coupled to a quadrupole mass spectrometer. The advantages of this technique are that the parent molecules spend a very short time in the pyrolysis zone (20−30 μs) and that the subsequent expansion permits the stabilization of thermal products that are not observable using conventional pyrolysis methods. A detailed analysis of the mass spectra as a function of pyrolysis temperature revealed the participation of five thermal decomposition channels. *Ab initio* calculations on the stable structures and transition states of the azidoacetone system in combination with an analysis of the dissociative ionization pattern of each channel allowed the identity and mechanism of each channel to be elucidated. At low temperatures (296−800 K) the azide decomposes principally by the loss of N_2 to yield the imine ($CH_3COCHNH$), which can further decompose to CH_3CO and CHNH. At low and intermediate temperatures a process involving the loss of N_2 to yield CH_3CHO and HCN is also open. Finally, at high temperatures (800−1250 K) a channel in which the azide decomposes to a stable cyclic amine ($CO(CH_2)_2NH$) (after loss of N_2) is active. The last channel involves subsequent thermal decomposition of this cyclic amine to ketene (H_2CCO) and methanimine (H_2CNH).

1. Introduction

The decomposition of azides with the release of N_2 provides the basis of their use in a large number of applications. For example, due to the exothermicity of its decomposition and liberation of gaseous N_2 sodium azide is commonly used in automobile air-bags.[1] Covalent organic azides, on the other hand, are extensively used in peptide chemistry, combinatorial chemistry, and heterocyclic synthesis.[2] Furthermore, azides are increasingly used in chemical vapor deposition for the generation of nitride films.[3] Therefore, a detailed understanding of their decomposition is of great interest.

The thermal decomposition of a range of organic azides has been extensively studied by Dyke and co-workers[4−8] using pyrolysis in combination with UV photoelectron spectroscopy and a matrix-isolation IR technique together with *ab initio* molecular orbital methods. Two principal mechanisms of thermal decomposition were invoked by these authors, the first of which involved the loss of N_2 with the formation of the imine ($RCH_2N_3 \rightarrow RCHNH + N_2$). This mechanism was originally proposed by Bock and Dammel[9−11] to explain the thermal decomposition of a series of alkyl azides. Whether the singlet nitrene ($^1RCH_2N$) rearranges to the imine form (^1RCHNH) by a 1,2 H-atom shift synchronous with the nitrogen elimination or whether the singlet nitrene is first formed followed by a 1,2 H-atom shift is still a matter of debate in the literature.[12−16]

The second type of dissociation mechanism proposed by Dyke and co-workers involved the formation of cyclic transition states in which a proton or an alkyl group is transferred from a remote site in the molecule to the electron deficient N atom. The first molecule for which this mechanism was proposed was 2-azidoacetic acid[4] where the mechanism shown in Scheme 1 was proposed.

In their experiments the simultaneous ejection of N_2 and formation of CO_2 led the authors to conclude that the above mechanism was the most important decomposition pathway. No evidence was found for the formation of imine *via* a 1,2 H-atom shift.

Subsequently, this mechanism type was also proposed to explain the decomposition products of ethyl azidoacetate (N_3CH_2COOEt),[6] methyl azidoformate (N_3COOMe),[8] and ethyl azidoformate (N_3COOEt).[8] Clearly in the case of the latter two molecules the 1,2 H-atom shift is not possible as there is no hydrogen atom on the carbon α to the azido group. On the other hand, the experimental results on the thermal decomposition of 2-azidoethanol ($N_3CH_2CH_2OH$),[6] 2-azidoacetamide ($N_3CH_2CONH_2$),[7] and 2-azido-*N*,*N*-dimethylacetamide ($N_3CH_2CONMe_2$)[8] were found to proceed *via* a 1,2 H-atom shift followed by thermal decomposition of the subsequently formed imine.

The innovative aspect of the technique used in this work with respect to conventional pyrolysis methods is given by the short

* To whom correspondence should be addressed at Università La Sapienza. E-mail: domenico.stranges@uniroma1.it.
† Università "La Sapienza".
‡ Departamento de Química, Faculdade de Ciências e Tecnologia, Universidade Nova de Lisboa.
§ Departamento de Física, Faculdade de Ciências e Tecnologia, Universidade Nova de Lisboa.
# ISMN-CNR, Sez. Roma 1.

10.1021/jp077406j CCC: $40.75
Published on Web 03/15/2008

SCHEME 1

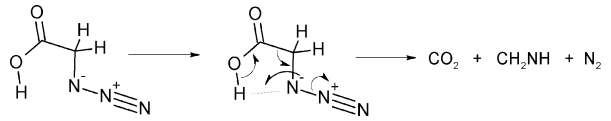

residence time of the parent molecule in the pyrolysis zone (20−30 μs) together with the internal cooling of the nascent thermal products on their exit from this region through a supersonic expansion. Therefore, in the case of pyrolysis of organic molecules, which proceeds *via* stepwise mechanisms, it is possible to isolate intermediate thermal decomposition products that are not observed using conventional oven techniques, providing a more detailed insight into the mechanisms involved. These aspects are demonstrated in this work by the study of azidoacetone. This molecule was chosen because both mechanisms outlined above have been invoked to account for the various pyrolysis products observed[5,6] and therefore provides the ideal testing ground for the method. This study also contains an extensive computational analysis of the dissociation mechanisms to provide further information on the competing decomposition channels.

2. Experimental Section

Azidoacetone was prepared as described in ref 5. The measurements were carried out using a molecular beam apparatus (at the University of Roma "La Sapienza") that has been described in detail previously.[17] Briefly, a mixture of 1 % N_3-CH_2COCH_3 seeded in Helium carrier gas was passed through a piezoelectrically activated pulsed valve[18] operated at a repetition rate of 100 Hz. The gas mixture was then expanded through a resistively heated SiC tube (length 23 mm) inducing the thermal decomposition of the molecule under examination. At the exit of the SiC tube the gas undergoes a free jet expansion, resulting in internal cooling of the thermal decomposition products, which are thus stable to further dissociation during their flight time to the electron impact ionizer. The product gas jet is then doubly skimmed and flies a distance of 40 cm to a differentially pumped home-built electron bombardment analyzer. Liquid nitrogen cooling of the analyzer allowed the background pressure in the ionization chamber to be held at $<1.0 \times 10^{-11}$ mbar, thus minimizing the effect of ionization of the background gas. The ionizer was operated at an electron energy of 100 eV and the resulting ions were mass analyzed by coupling to a quadrupole mass spectrometer (Extrel 150-QC) and a Daly type ion counter.

Electron impact mass spectra were recorded as a function of the heating current passed through the SiC tube. To be able to convert the electrical power applied to the SiC tube to temperature, the velocity of a neat Helium jet was measured as a function of the electrical power passing through the SiC tube. These measurements were performed by inserting a spinning slotted disk (200 Hz) into the molecular beam and measuring the flight time for a "slice" of the He atoms in the beam. The velocity of a supersonic ideal atomic gas jet can be related to the temperature of the source (*i.e.*, the temperature of the pyrolysis tube) *via* the expression $T = (mv^2/5R)$, where T is the source temperature, m is the mass of gas, v is the velocity of the beam, and R is the gas constant.[19]

3. Computational Details

Ab initio calculations were carried out using the Gaussian03W program.[20] The geometries of stable structures were optimized at the hybrid B3LYP density functional[22] level of theory using the split valence plus polarization 6-31G(d) basis set. The hybrid B3LYP functional was chosen because of its ability to accurately describe the geometries of transition states.[23] Isomerization and dissociative transition states were optimized using the analytic gradient procedure and the combined synchronous transit and quasi-Newton (STQN) method.[24] All transition states were confirmed to be true transition states by performing a frequency analysis on the relevant geometry to demonstrate that there was only one imaginary frequency for each struture.

Single-point G3(MP2)//B3LYP calculations[25] were also performed on all of the structures identified, resulting in energies that approximate a QCISD(T,FC)/G3MP2large//B3LYP/6-31G-(d) calculation. This composite method involves a frequency analysis at the B3LYP/6-31G(d) level to take into account the zero point energies, a single-point energy calculation using the multireference QCISD(T) method to estimate the effects of correlation and an MP2/G3MP2Large calculation to estimate the effects of a limited basis set. This method was chosen as a compromise between minimizing CPU time and maximizing the accuracy of single-point calculations capable of comparing energies of stable, transition state and radical structures.

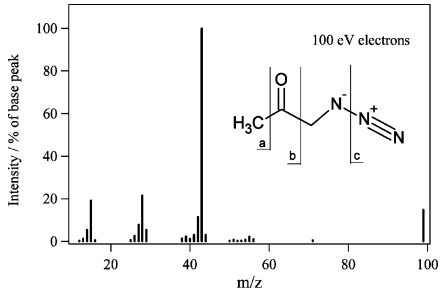

Figure 1. Electron impact spectra of room temperature azidoacetone at an electron energy of 100 eV.

4. Results and Analysis

4.1. Electron Impact Mass Spectra of Room Temperature Azidoacetone. Figure 1shows the electron impact mass spectrum of azidoacetone with an electron energy of 100 eV. This spectrum was recorded following expansion of the target molecule through the SiC tube with no heater current and therefore at a temperature of 296 K. The contribution to the spectra due to electron impact ionization and dissociative ionization of the background gas was subtracted by recording mass spectra under identical conditions in which the molecular beam was prevented from entering the ionization region by a beam block. The spectra are also corrected for the transmission curve of the quadrupole mass spectrometer.

A mass spectrum was also recorded with the more standard electron energy of 70 eV. The resulting spectrum was almost identical to that shown in Figure 2 with only very minor differences due to slightly increased fragmentation at the higher electron impact energy as would be expected. Comparing the ionization pattern obtained in this work to that observed by Duarte *et al.*[21] shows that there are significantly less light fragments in the present work. Indeed, the above authors noted in their discussion that their electron impact spectra were likely to be modified by the contribution from the ionization of thermal decomposition species. In contrast, the spectrum shown in this work was obtained by a free jet expansion of the parent molecule at room temperature, and therefore no thermal decomposition occurs prior to ionization. Furthermore, the parent molecules are internally cold when they reach the ionization region due to the expansion properties of the supersonic jet.

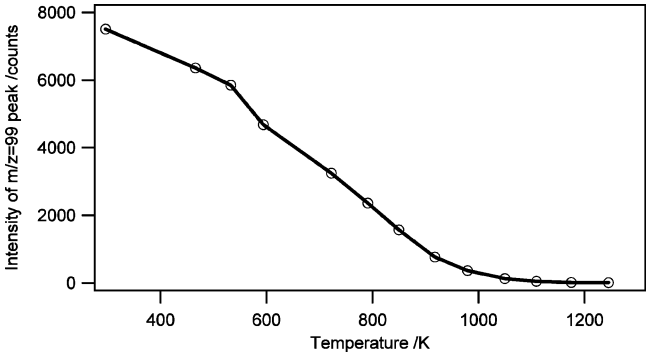

Figure 2. Intensity of the $m/z = 99$ peak in the mass spectrum of pyrolyzed $N_3CH_2COCH_3$ as a function of the pyrolysis temperature.

The main peaks in the spectra are $m/z = 15$, 28, 43, and 99, which can be easily related to the fragmentation channels shown in the inset of Figure 1 where channel a yields $m/z = 15$ ions, channel b $m/z = 43$ fragment ions, and channel c $m/z = 28$ fragment ions.

4.2. Analysis of Mass Spectra as a Function of Pyrolysis Temperature. A series of mass spectra were recorded with an electron energy of 100 eV in which the temperature of the SiC tube was varied by changing the current flowing in the tube from 0 to 2.5 A in steps of ~0.2 A. Using the calibration described in the experimental section, we showed that this current range corresponds to a temperature range of the SiC tube from 296 to 1250 K. This temperature will be the same for all internal degrees of freedom of the molecules if thermal equilibrium is reached during the residence time of the molecules inside the hot region (20−30 μs). Under our conditions it is likely that the rotational and translational degrees of freedom will reach equilibrium due to their fast relaxation rates. The vibrational relaxation rates, on the other hand, are slower, and therefore, it could be possible that the residence time in the hot region is not sufficient to reach thermal equilibrium for these degrees of freedom. In this case the temperature measured by the neat helium beam calibration will represent an upper limit for the vibrational temperature. It should be noted that it is the vibrational energy that drives the dissociation processes and in this context we will continue to use the term "thermal decomposition" to describe these processes.

Figure 2 shows a plot of the intensity of the $m/z = 99$ peak as a function of the temperature of the pyrolysis tube. From this figure it is clear that the number of parent molecules surviving the passage through the pyrolysis region decreases rapidly with temperature due to thermal decomposition of the azide. Furthermore, it can be seen that at pyrolysis temperatures ≥1100 K no parent azide molecules survive; *i.e.*, thermal decomposition of the parent molecule is complete. Conversely, the intensity of the peaks corresponding to lower masses increase due to the larger number of thermal decomposition products reaching the detector.

Indeed, it was possible to remove the contribution of the dissociative ionization of the unpyrolysed parent molecule to the total mass spectrum at each pyrolysis temperature. This was done by normalizing the spectrum in Figure 1 to the relative intensity of the $m/z = 99$ peak and subtracting the resulting spectrum from the total mass spectrum at each pyrolysis temperature. In this way, it was possible to obtain the mass spectrum of the thermal decomposition products as a function of the pyrolysis temperature. At room temperature no thermal decomposition occurs and, therefore, the intensity of the peaks in the mass spectrum corresponding to the thermal decomposition products is zero. With increasing temperatures the intensity

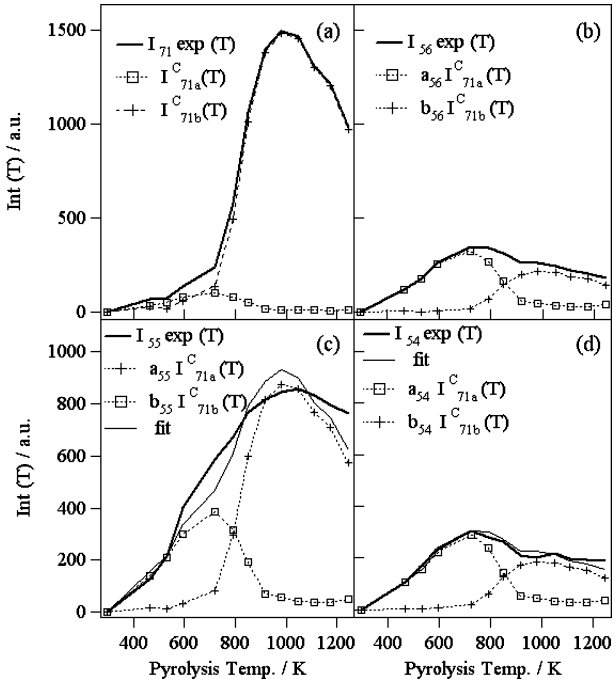

Figure 3. Fits to the temperature dependence of the intensity of the m/z = (a) 71, (b) 56, (c) 55, and (d) 54 peaks in the mass spectra of the thermal decomposition products of azidoacetone (see text). It should be noted that the fitted curves in (a) and (b) reproduce exactly the experimental data and are therefore not shown in those plots.

of these peaks increase but in characteristic ways for each mass. The bold lines in Figure 3 present an illustration of this behavior for the $m/z = 71$, 56, 55, and 54 peaks. We consider that the last three of these ion peaks are due to dissociative ionization fragmentation of the neutral mass 71 thermal products produced in the pyrolysis of azidoacetone (see discussion). It can be seen that the $m/z = 71$ peak initially increases very slowly but then rapidly beginning at 800 K and the $m/z = 56$ peak increases rapidly starting from 300 K but then decreases in intensity at higher pyrolysis temperatures.

These observations can be explained if it is concluded that there are two thermal decomposition processes that yield two distinct mass 71 fragments: one channel that starts to operate at low temperatures and the other at higher temperatures. The different temperature dependencies of the various m/z peaks can then be explained by varying contributions of the two channels due to their characteristic dissociative ionization patterns in the electron impact ionizer. These concepts can be expressed in mathematical form as follows:

$$I_{71}(T) = I^{C}_{71a}(T) + I^{C}_{71b}(T) \quad (1)$$

$$I_{56}(T) = a_{56}I^{C}_{71a}(T) + b_{56}I^{C}_{71b}(T) \quad (2)$$

where $I_{71}(T)$ and $I_{56}(T)$ represent the intensity of the $m/z = 71$ and 56 peaks as a function of the pyrolysis temperature, $I^{C}_{71a}(T)$ and $I^{C}_{71b}(T)$ are the basis sets that describe the intensity behavior of the two thermal dissociation channels producing mass 71 fragments as a function of the pyrolysis temperature and a_{56} and b_{56} are the coefficients that describe the probability of dissociative ionization fragmentation of the two channels to the $m/z = 56$ ion. To determine the $I^{C}_{71a}(T)$ and $I^{C}_{71b}(T)$, the experimental temperature variations of the intensity of the $m/z = 71$ and 56 peaks were fit by means of a genetic algorithm to the above formulas and the results of these fits are shown in Figure 3a,b.

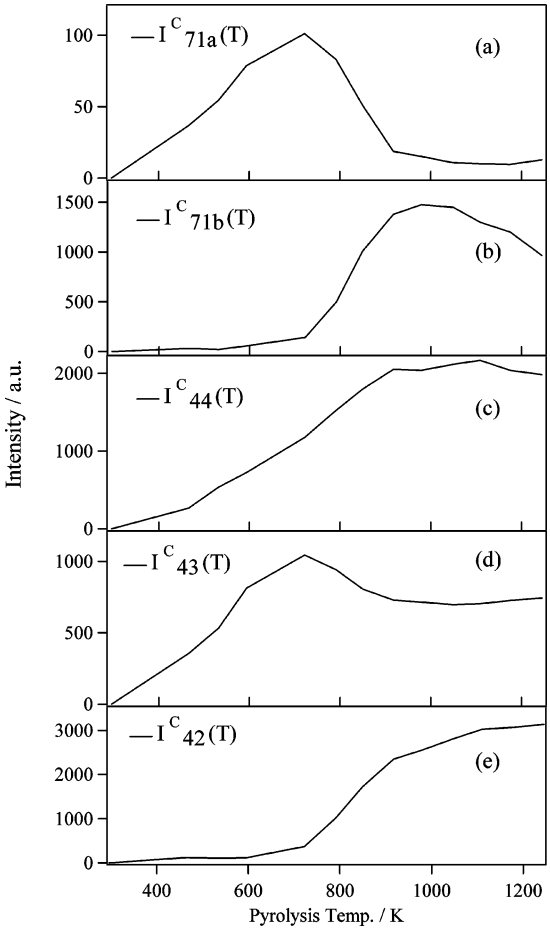

Figure 4. Basis sets extracted from the fitting process that best describe the intensity dependence of the thermal decomposition process of the azidoacetone producing parent thermal products of masses 71 (a) and (b), 44 (c), 43 (d), and 42 (e) (see text for details).

Having extracted the intensity behavior of the two decomposition channels (shown in Figure 4a,b) it was then possible to fit the intensity behaviors of the $m/z = 52$, 53, 54, and 55 peaks using the analogous expression for those masses:

$$I_M(T) = a_M I^C_{71a}(T) + b_M I^C_{71b}(T) \quad (3)$$

where $I_M(T)$ represents the intensity of the $m/z = M$ peaks as a function of the pyrolysis temperature and a_M and b_M are the coefficients that describe the dissociative ionization fragmentation patterns of the two channels. Therefore, this fitting process yields the a_M and b_M coefficients corresponding to each of these masses. An example of these fits are shown in Figure 3c,d for the $m/z = 55$ and 54 peaks, respectively.

Clearly, the thermal products of these two channels can also fragment to lower masses in the ionizer. However, following the measurements of Dyke *et al.*[5] who observed CH_3CHO ($m/z = 44$) and CH_2CO ($m/z = 42$) and also postulated the formation a mass 43 fragment, we consider that three other channels yielding thermal deomposition products with masses of 44, 43, and 42 (which correspond to the CH_3CHO, CH_3CO, and CH_2-CO product channels, respectively; see Discussion) are also active in addition to the two channels with mass 71 parent fragments. At this point it was assumed that the $m/z = 44$ peak in the mass spectrum can only be observed as a direct thermal product of the pyrolysis of the azidoacetone (and thus not as a result of dissociative ionization of the mass 71 products in the ionizer).

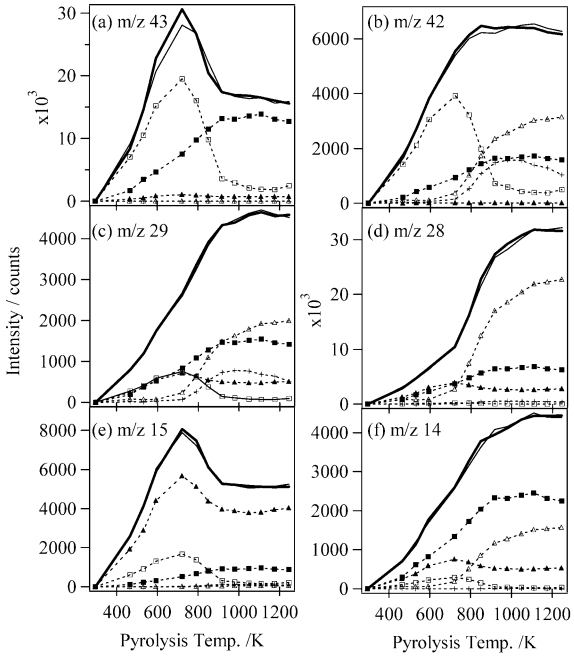

Figure 5. Fits to the temperature dependence of the m/z = (a) 43, (b) 42, (c) 29, (d) 28, (e) 15, and (f) 14 peaks in the mass spectra of the thermal decomposition products of azido acetone. The experimental dependence of each mass is illustrated by a full bold line, the total fit by the thin full line, and the contributions of each of the thermal decomposition channels are shown by dotted lines with the following symbols: □, channel 71a; +, channel 71b; ■, channel 44; ▲, channel 43; △, channel 42.

Therefore, the intensity variation of the $m/z = 44$ peak was taken to be the basis set for the dependence of the intensity of this channel with the pyrolysis temperature. The intensity behavior of the m/z peaks 12, 13, 14, 15, 16, 26, 27, 28, 29, 40, 41, 42, and 43 were then fit in a global manner to the following formulas with a genetic algorithm:

$$I_M(T) = a_M I^C_{71a}(T) + b_M I^C_{71b}(T) + c_M I^C_{44}(T) + d_M I^C_{43}(T) + e_M I^C_{42}(T) \quad (4)$$

where the free parameters in the fitting process are the parameters a_M to e_M describing the dissociative ionization fragmentation pattern of each channel and the basis sets describing the temperature variation of the thermal dissociation channels producing mass 43 and 42 products: $I^C_{43}(T)$ and $I^C_{42}(T)$. A global fit of all experimental temperature variation patterns $m/z = 12-43$ in which each m/z peak was weighted by its intensity was performed. Figure 5 shows a selection of these fits for the most intense m/z peaks, and the basis sets describing the temperature variation of the thermal decomposition channels producing $m/z = 44$, 43, and 42 fragments are shown in Figure 4c−e, respectively. Finally, the fragmentation patterns for each thermal decomposition channel (*i.e.*, for all products of a given channel) obtained in the form of the a_M to e_M coefficients are plotted in Figure 6 where the heaviest parent fragment intensity of each channel have been normalized to 1.

5. Discussion

5.1. Thermal Decomposition Channels Yielding Fragments with Mass 71. The formation of thermal decomposition products of 2-azidoacetone with mass 71 corresponds to the loss of N_2. From the above results it is clear that there are two distinct channels that produce mass 71 fragments with significantly

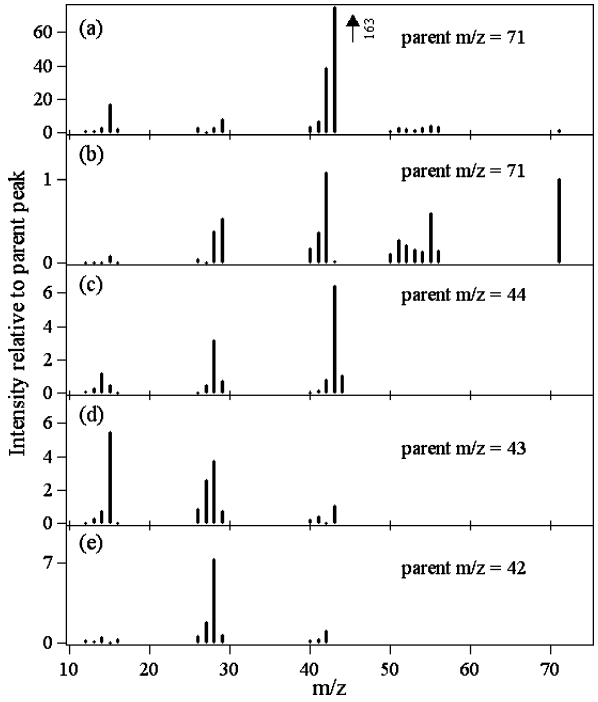

Figure 6. Dissociative ionization pattern for the thermal decomposition processes of azidoacetone in which the heaviest parent fragment masses are (a) and (b) 71, (c) 44, (d) 43, and (e) 42 amu. These patterns were obtained with an electron energy of 100 eV (see text).

SCHEME 2

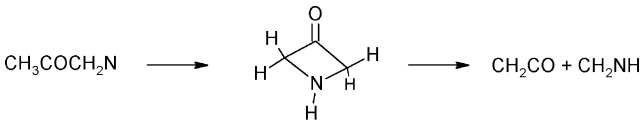

different dissociative ionization patterns in the ionizer. Although Dyke *et al.*[5] did not directly observe any thermal products with mass 71, they proposed a multistep process in which the first step consists of the formation of the nitrene by loss of N_2:

$$CH_3COCH_2N_3 \rightarrow CH_3COCH_2N + N_2 \qquad (5)$$

As a possible explanation of their observation of CH_2CO and CH_2NH, they suggested that the nitrene could decompose through a strained cyclic intermediate into ketene and methanimine (see Scheme 2).

Furthermore, they suggested a second channel in which the initially formed nitrene rearranges to the corresponding imine *via* a 1,2 H-atom shift followed by a radical chain reaction that could produce the other thermal products observed in their study: CH_3CHO, CH_2NH, HCN, CO, etc.

From the results of the present study it seems clear that indeed both of these channels are operative with one of the channels being dominant at low temperatures whereas the other is open at higher temperatures. Examination of the dissociative ionization patterns of the two channels helps to identify the nature of the fragments. The channel producing mass 71 fragments that dominates at low temperatures exhibits strong dissociative ionization, as can be seen from the mass spectrum for this channel illustrated in Figure 7a, where the parent *m*/*z* peak can be seen to be very weak with respect to the $m/z = 15$, 42, and 43 peaks. This strongly suggests that this channel corresponds to formation of the imine where the $m/z = 43$ and 15 fragment ions could be formed by simple cleavage of the carbon−carbon bonds α to the carbonyl group, as illustrated by the fragment patterns a and b shown in Scheme 3.

The high temperature mechanism (see Figure 4b), on the other hand, shows a completely different fragmentation pattern in the ionizer (Figure 6b), in particular with a very intense parent peak. This suggests that this fragment is more stable to dissociative ionization with respect to the imine, as may be expected for the cyclic mass 71 fragment in which at least two bonds must be broken to produce the lower mass ions. Also, the peaks in the range $m/z = 50-56$ are relatively more intense. This can be explained by the fact that dissociative ionization processes that lead to these masses involve the initial loss of neutral NH, CH_2, or O. In all of these cases either two bonds or a double bond must be broken and hence less energy is available for subsequent decomposition of the ions produced in these processes. This leads to a relatively large intensity of these peaks for this channel. Furthermore, inspection of Figure 6b reveals that $m/z = 42$ and 29 peaks are prominent in this spectrum. This is consistent with dissociative ionization of the cyclic fragment by breaking the carbon−carbon bond α to the carbonyl group and the diametrically opposite nitrogen−carbon bond, yielding two fragments of masses 42 amu (CH_2CO) and 29 amu (CH_2NH), which is analogous to the thermal decomposition shown in the second step of Scheme 3.

To corroborate these conclusions, *ab initio* calculations were performed on the stable structures and transition states involved in the thermal decomposition of azidoacetone. The geometries of these states were optimized at the B3LYP/6-31G(d) level and then high accuracy single-point energy calculations were performed on each geometry using the G3(MP2)//B3LYP composite method (see the section on computational details). The resulting energies and optimized geometries are shown in Figures 7 and 8, respectively. As can be seen from Figure 8a,b, the ground state azidoacetone exists in two conformers that can be differentiated by whether the azide group is gauche (Figure 8a) or anti (Figure 8b) to the carbonyl group. The energy difference between these structures is very small (0.4 kcal/mol), and a relaxed scan on the PES of the molecule while varying the NNCC dihedral angle followed by a G3(MP2)B3 single-point energy calculation on the transition state structure showed that the barrier to interconversion between the gauche and anti forms is 3.9 kcal/mol. Therefore, even at low temperatures there is a free interchange between these structures.

Following the loss of N_2 the most stable structure, which can be assumed by the remaining moiety, is the imine form (Figure 8c,d). The imine can also exist in two conformer structures, in this case, depending on whether the NH group is gauche (Figure 8c) or anti (Figure 8d) with respect to the carbonyl group. Again the energy difference between these two structures is small (0.8 kcal/mol) and a relaxed scan of the PES followed by optimization of the geometry of the resulting transition state and a G3(MP2)B3 calculation of its energy revealed a barrier of 4.8 kcal/mol for the gauche → anti interconversion. The energies of the imine structures plus molecular nitrogen are more than 50 kcal/mol more stable than the parent azide, and therefore, the decomposition is a strongly exothermic process.

The most stable transition state identified between the azide and imine forms is that shown in (Figure 8g) and is referred to as TS1 in Figure 7. An intrinsic reaction coordinate (IRC)[26] calculation was performed at the B3LYP/6-31G(d) level to ensure that this TS is indeed the state that connects the desired reactants and products. Initially as the breaking N−N bond is elongated the potential energy increases until the transition state is reached, as expected. At this point, however, further elongation of this N−N bond is concurrent with movement of one of the H atoms on the carbon atom nearest the terminal nitrogen

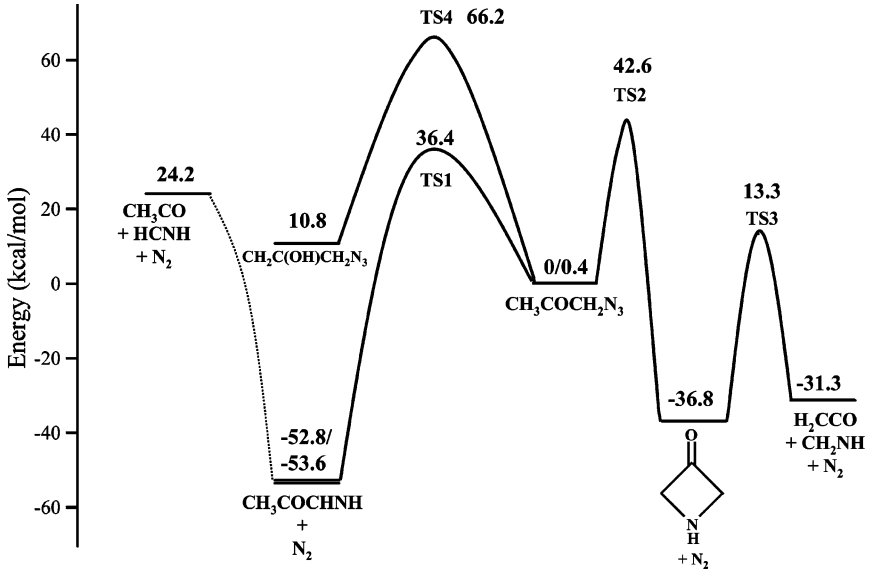

Figure 7. Potential energy barriers for the pyrolysis of the $CH_3COCH_2N_3$ system, determined at the G3(MP2)B3 level.

SCHEME 3

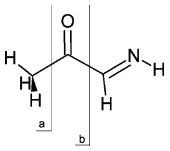

atom. At a breaking N−N bond distance of approximately 2.5 Å the potential energy rapidly drops as the imine is formed by a 1,2 H-atom shift to the terminal nitrogen atom. At this level of theory there is no minimum in the potential energy path between the transition state and the point at which the 1,2 H-atom shift occurs, thus indicating that the singlet nitrene (^{1}-CH_3COCH_2N) is not stable to rearrangement. Single-point energy calculations using the G3(MP2)B3 composite method resulted in a barrier height of 36.4 kcal/mol for this transition state.

The next transition state to consider is one in which a hydrogen atom is transferred from a more remote site in the molecule to the electron deficient terminal nitrogen atom formed by the loss of N_2. This type of mechanism, originally proposed by Dyke *et al.*,[5,6] provides another way in which the singlet nitrene that would result from direct loss of the N_2 can be stabilized. *Ab initio* calculations on the cyclic structure suggested by Dyke *et al.*[5,6] revealed a surprisingly stable structure for the four-membered ring (see Figure 8e) that is almost 40 kcal/mol more stable than the parent azide. The transition state that links this cyclic state to the parent azide was also identified and is referred to in this work as TS2 (see Figure 8h). Again an IRC calculation was performed to confirm that this transition state connects the parent azide to the cyclic structure. It can be seen that this TS consists of a five-membered ring in which the H atom in the process of being transferred from the CH_3 group to the N atom is shared between these two groups. The single-point energy calculation on this TS resulted in a barrier height of 42.6 kcal/mol.

At this point it would seem quite clear that the calculations can provide a qualitative explanation for the two thermal decomposition channels resulting in two different mass 71 products. The channel that is open at low temperatures corresponds to the decomposition through the TS1 state (barrier height 36.4 kcal/mol) to form the imine, and the mechanism that opens at higher temperatures is a result of thermal

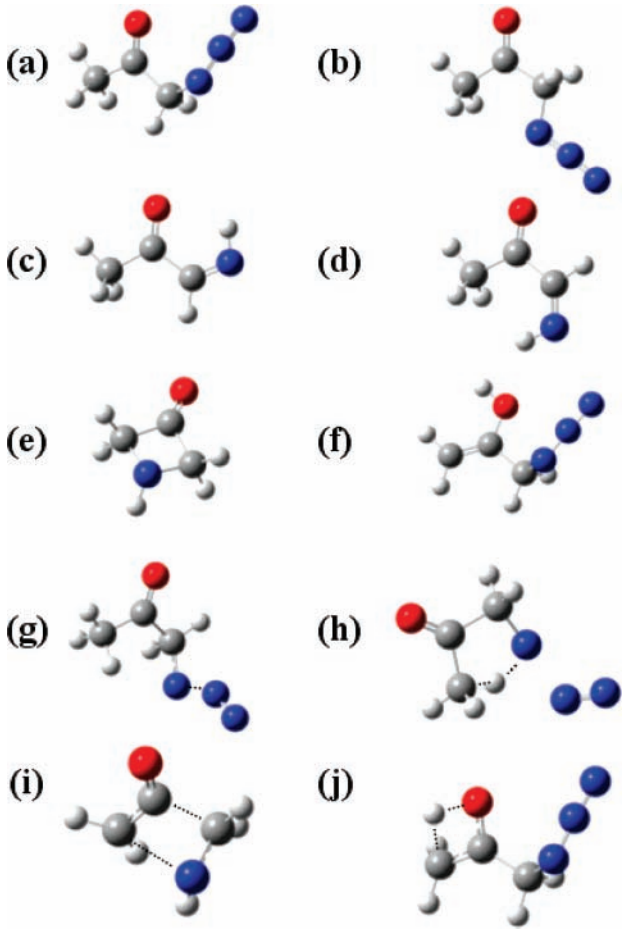

Figure 8. Optimized geometries (at the B3LYP/6-31G(d) level) of the stable molecules and transition states shown in Figure 7. (a) and (b) are the gauche and anti conformers of the azidoacetone. (c) and (d) are the gauche and anti conformers of the imine produced after loss of N_2 from the azidoacetone. (e) is the cyclic structure that can result from ring close after loss of N_2 from the azidoacetone, and (f) is the enol structure resulting from keto-enolization of the parent. (g), (h), (i), and (f) represent the structures of transition states TS1, TS2, TS3, and TS4, respectively.

decomposition through TS2 (barrier height 42.6 kcal/mol) leading to the cyclic state. This result is consistent with the conclusions made on the dissociative ionization patterns of these

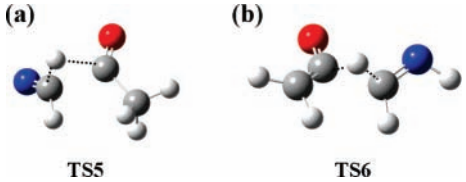

Figure 9. Transition state geometries optimized at the B3LYP/6-31G-(d) level (see text for details).

SCHEME 4

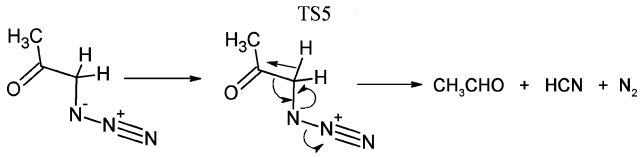

two channels. Both of these thermal fragments are relatively stable to further fragmentation; however, with an increase in temperature, the imine and cyclic structure can further decompose, resulting in a decrease in the efficiency of both channels at high temperatures, as will be discussed in the following section.

5.2. Thermal Decomposition Channels Yielding Fragments with Masses 44, 43, and 42 amu. Examination of the temperature dependence of the lower mass fragment channels (see Figure 4) reveals certain similarities between the behaviors of the *m*/*z* 43 and *m*/*z* 71a (which from the above discussion has been identified as the imine channel) channels and the *m*/*z* 42 and *m*/*z* 71 b (identified as the cyclic fragment channel) channels. These similarities can be rationalized by considering the possible fragmentation mechanisms of the two mass 71 thermal fragments (see below). The temperature behavior of the mass 44 channel, on the other hand, appears to be different from all of the other processes in that it gradually rises at low temperatures and then plateaus in the range from 900 to 1200 K. These observations suggest that the thermal decomposition process yielding mass 44 fragments proceeds through a transition state that is independent of the transition states leading to mass 71 fragments. Indeed, Dyke *et al.*[5,6] suggested a single-stage three-body decomposition in which a 1,2 H-atom shift takes place from the CH_2 group α to the carbonyl group to the carbon atom of the carbonyl group, yielding CH_3CHO, HCN, and N_2. This mechanism is shown in Scheme 4.

The search for a transition state consistent with such a mechanism yielded the structure shown in Figure 9a, *i.e.*, TS5. The height of the potential energy barrier of this transition state, calculated at the G3(MP2)B3 level, is 37.6 kcal/mol, which lies between the barrier heights of transition states TS1 and TS2. This result explains the intermediate temperature behavior of this channel with respect to the temperature dependence of the channels proceeding through TS1 and TS2.

The similarity of the temperature variation of the mass 43 channel to that of the low temperature mass 71 channel suggests that the initial step in the formation of the mass 43 fragment is the formation of the imine. To explain these observations we propose that the identity of the mass 43 thermal fragment is the CH_3CO radical formed by further thermal decomposition of $CH_3COCHNH$. The partner fragment in this decomposition is also a radical: CHNH. A relaxed potential energy scan at the B3LYP/6-31G(d) level in which the relevant carbon−carbon bond was progressively lengthened revealed that there is no barrier in the exit channel of this process. The energy of the asymptote of this channel lies at 24.2 kcal/mol with respect to the parent azide. Dyke *et al.*[5] suggested another mechanism that

SCHEME 5

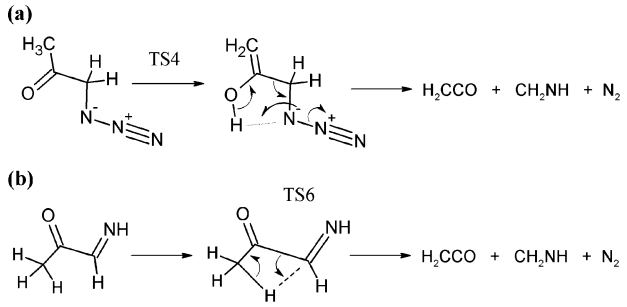

could give rise to a mass 43 fragment (CH_3NCH_2). This mechanism involves the migration of the methyl moiety α to the carbonyl group to the terminal N atom (after loss of N_2), yielding simultaneously N_2, CO, and CH_3NCH_2. A computational search for the transition state involved in this mechanism was not successful, and therefore, this mechanism cannot be excluded as a possible open channel.

The final thermal decomposition channel to be explained is that which yields the mass 42 fragment. The most plausible identity of this fragment is ketene (H_2CCO), which would be formed with the partner fragment methanimine (H_2CNH). However, there are a number of mechanisms that can yield these fragments. As mentioned above, the temperature dependence of this channel is similar to that of the thermal decomposition channel that proceeds through TS2. Indeed, the cyclic amine can decompose by cleavage of two bonds passing through the transition state shown in Figure 8i and is denoted as TS3 in this work. The height of the barrier leading to these products is 13.3 kcal/mol with respect to the parent azide. We propose that this mechanism accounts for the production of ketene and methanimine; however, it is necessary to examine the other possible mechanisms that can lead to these products (illustrated in Scheme 5) before this conclusion can be considered the only valid one.

The first of these mechanisms (see Scheme 5a), which involves as the first step a keto-enolization of the azidoacetone, was suggested by Dyke *et al.*[5,6] as a possible source of ketene and methanimine. Optimization of the transition state structure for keto-enolization (TS4) and calculation of its energy yielded a barrier height of 66.2 kcal/mol for this process. This barrier is much higher than those of TS1, TS2, and TS5, and therefore, it can be concluded that this channel is not operative.

The second mechanism (shown in Scheme 5b), which involves the fragmentation of the imine through TS6 (see Figure 9b), was also investigated from a computational point of view. In this case the barrier height calculated using the same proceedure as that used for the other transition states was found to be 31.6 kcal/mol, which is 7.4 kcal/mol higher than the asymptotic energy of the radical decomposition channel yielding CH_3CO and CHNH. Therefore, it is clear that the imine decomposition occurs preferentially *via* the radical channel. As a result it can be concluded that the mass 42 channel takes place by successive passage through TS2 and TS3.

Having identified the nature of the channels involved in the thermal decomposition we can now proceed to a discussion of the temperature dependence of each channel. In particular, we concentrate on the "linked" channels, *i.e.*, the mechanisms proceeding through TS1 (to form the imine) followed by radical−radical dissociation and that which involves successive passage through TS2 an TS3. At room temperature no thermal decomposition takes place but as soon as the temperature is raised some molecules decompose by passage through TS1.

However, temperature is not the only variable that needs to be considered in this case but also the position within the pyrolysis tube at which the decomposition event takes place. At low temperatures, on average, it is probable that the thermal decomposition takes place near the end of the tube, thus allowing little time for further decomposition of the products to take place. As the temperature is increased, also the average position within the tube where the decomposition takes place gradually moves toward to the beginning of the tube. This reasoning explains why at high temperatures the intensities of the imine products decrease to nearly zero (see Figure 6a) and that of the radical/radical dissociation channel reaches a plateau (see Figure 6c). Similar reasoning can be applied to the mechanisms proceeding through TS2 (formation of the cyclic amine) and TS3 (decomposition of the cyclic amine) but with the temperature dependence shifted to higher temperatures due to the higher barrier for TS2 with respect to TS1.

6. Conclusions

2-Azidoacetone ($CH_3COCH_2N_3$) was synthesized and its thermal decomposition products were characterized experimentally using flash pyrolysis in combination with a molecular beam/mass spectrometric technique. The experimental results demonstrated the participation of no less than five thermal decomposition channels and yielded both the temperature dependence of these channels in the range 296−1250 K and the dissociative ionization pattern of the thermal decomposition products associated with each of these channels at an electron ionization energy of 100 eV. Examination of these experimental data together with a computational analysis of the azide/imine system allowed the identification of the mechanisms leading to each channel. Two low temperature (296−800 K) mechanisms are associated with the loss of N_2 with a 1,2 H-atom shift to yield the imine ($CH_3COCHNH$) fragment, which can either survive the passage through the pyrolysis region and yield a mass 71 fragment or undergo further fragmentation *via* a radical−radical decomposition channel to CH_3CO (mass 43 amu) and CHNH (mass 28 amu). An independent channel that can compete with the above channel at higher temperatures (750−1250 K) involves the formation of a stable cyclic amine ($CO(CH_2)_2NH$) with mass 71 amu, which can further fragment to ketene (H_2CCO) and methanimine (CH_2NH) by cleavage of two bonds. The products of the decomposition channel that yields the mass 44 fragments have been identified as CH_3CHO, HCN, and N_2. The mechanism yielding these products has an intermediate barrier height with respect to the first two processes and occurs *via* loss of N_2 with a 1,2 H-atom shift from the CH_2 group α to the carbonyl group to the carbon atom of the carbonyl group with simultaneous formation of HCN. The flash pyrolysis technique presents significant advantages with respect to conventional oven based pyrolytic methods in that the residence time of the target molecules in the pyrolytic region is much shorter and the subsequent expansion into a supersonic jet allows internal cooling of the nascent thermal decomposition fragments. The different experimental conditions utilized in the study of Dyke *et al.*,[5] in which the residence time of the azidoacetone molecules in the pyrolysis zone was estimated to be 3 ms[7] with respect to the residence times in this study (20−30 μs), explains why the mass 71 fragments were not observed in that work.

Acknowledgment. This research was supported by the Italian Ministero dell'Università e della Ricerca-MUR (PRIN 2005) and a Marie Curie Intra-European Fellowship within the sixth European Community Framework Programme (Contract No. MEIF-CT-2005-024895).

Supporting Information Available: Complete ref 20. Cartesian coordinates and absolute energies of all optimized critical structures. This information is available free of charge via the Internet at http://pubs.acs.org.

References and Notes

(1) Berger, J. M.; Butler, P. B. *Combust. Sci. Technol.* **1995**, *104*, 93.
(2) Brase, S.; Gil, C.; Knepper, K.; Zimmermann, V. *Angew. Chem., Int. Ed.* **2005**, *44*, 5188.
(3) Wang. J.; Gillan, E. G. *Thin Solid Films* **2002**, *422*, 62.
(4) Dyke, J. M.; Groves, A. P.; Morris, A.; Ogden, J. S.; Dias, A. A.; Oliveira, A. M.; Costa, M. L.; Barros, M. T.; Cabral, M. H.; Moutinho, A. M. *J. Am. Chem. Soc.* **1997**, *119*, 6883.
(5) Dyke, J. M.; Groves, A. P.; Morris, A.; Ogden, J. S.; Catarino, M. I.; Dias, A. A.; Oliveira, A. M.; Costa, M. L.; Barros, M. T.; Cabral, M. H.; Moutinho, A. M. *J. Phys. Chem. A* **1999**, *103*, 8239.
(6) Hooper, N.; Beeching, L. J.; Dyke, J. M.; Morris, A.; Ogden, J. S.; Dias, A. A.; Costa, M. L.; Barros, M. T.; Cabral, M. H.; Moutinho, A. M. *J. Phys. Chem. A* **2002**, *106*, 9968.
(7) Dyke, J. M.; Levita, G.; Morris, A.; Ogden, J. S.; Dias, A. A.; Algarra, M.; Santos, J. P.; Costa, M. L.; Rodriguez, P.; Barros, M. T. *J. Phys. Chem. A* **2004**, *108*, 5299.
(8) Dyke, J. M.; Levita, G.; Morris, A.; Ogden, J. S.; Dias, A. A.; Algarra, M.; Santos, J. P.; Costa, M. L.; Rodriguez, P.; Andrade, M. M.; Barros, M. T. *Chem. Eur. J.* **2005**, *11*, 1665.
(9) Bock, H.; Dammel, R.;Horner, L. *Chem. Ber.* **1981**, *114*, 220.
(10) Bock, H.; Dammel, R.; Aygen, S. J. *J. Am. Chem. Soc.* **1983**, *99*, 518.
(11) Bock, H.; Dammel, R. *J. Am. Chem. Soc.* **1988**, *110*, 5261.
(12) Arenas, J. F.; Marcus, J. I.; Lopez-Tocon, I.; Otero, J. C.; Soto, J. *J. Chem. Phys.* **2000**, *113*, 2282.
(13) Zeng, Y.; Sun, Q.; Meng, L.; Zheng, S.; and Wang, D. *Chem. Phys. Lett.* **2004**, *390*, 362.
(14) Jing, W.; Zheng, S.; Xinjiang, Z.; Xiaojun, Y.; Maofa, G.; Dianxun, W. *Angew. Chem., Int. Ed.* **2001**, *40*, 3055.
(15) Teslja, A.; Nizamov, B.; Dagdigian, P. J. *J. Phys. Chem. A* **2004**, *108*, 4433.
(16) Larson, C.; Ji, Y.; Samartzis, P.; Wodtke, A. M.; Lee, S. H.; Lin, J.; Chaudhuri, C.; Ching, T. T. *J. Chem. Phys.* **2006**, *125*, 133302.
(17) The appartus in Rome used in these experiments is very similar to that described in Stranges, D.; Stemmler, M.; Yang, X.; Chesko, J. D.; Suits, A. G.; Lee, Y. T. *J. Chem. Phys.* **1998**, *109*, 5372.
(18) Proch, D.; and Tickl, T. *Rev. Sci. Instrum.* **1989**, *60*, 713.
(19) Miller, D. R. in *Atomic and Molecular Beams* edited by G. Scoles (Oxford University Press, 1988).
(20) Frisch, M. J.; *et al. Gaussian 03*, revision B.01; Gaussian, Inc.: Pittsburgh, PA, 2003.
(21) Duarte, M. F.; Martins, F.; Fernandez, M. T.; Lanley, G. J.; Rodriguez, P.; Barros, M. T.; Costa, M. L. *Rapid Commun. Mass Spectrom.* **2003**, *17*, 957.
(22) Becke, A. D. *J. Chem. Phys.* **1992**, *97*, 9173. Becke, A. D. *J. Chem. Phys.* **1993**, *98*, 5648. Lee, C.; Yang, W.; Parr, R. G. *Phys. Rev.* **1988**, *B37*, 785.
(23) Durant, J. L. *Chem. Phys. Lett.* **1996**, *256*, 595.
(24) Peng, C.; Ayala, P. Y.; Schlegel, H. B.; Frisch, M. J. *J. Comput. Chem.* **1996**, *17*, 49.
(25) Baboul, A. G.; Curtiss, L. A.; Redfern, P. C.; Raghavachari, K. *J. Chem. Phys.* **1999**, *110*, 7650.
(26) Gonzales, C.; Schlegel, B. H. *J. Chem. Phys.* **1989**, *90*, 2154.